Design of Miniaturized Microstrip LPF and Wideband BPF With Ultra-Wide Stopband

Jin Xu, Yu-Xue Ji, Wen Wu, *Senior Member, IEEE*, and Chen Miao, *Member, IEEE*

***Abstract*—This letter presents a novel lowpass filter (LPF) structure which consists of a section of high-impedance microstrip line (HIML) with a pair of radial stubs (RSs) loaded at its center and a pair of stepped-impedance open stubs (SIOSs) loaded on both ends of HIML. The RSs loaded HIML exhibits a lowpass property and has a wide stopband. The loaded SIOSs not only can improve the roll-off rate of LPF significantly but also is able to extend the stopband. Based on such a LPF structure, a pair of highpass shorted HIMLs are paralleled on both sides of LPF to construct a wideband bandpass filter (BPF) with wide stopband. To validate the proposed method, two filters, i.e., a LPF with cutoff frequency f_c at 1.07 GHz and a BPF centered at $f_0 = 0.89$ GHz with -3 dB fractional bandwidth of 87%, are designed and fabricated. The measured results show the fabricated LPF has a -20 dB isolation bandwidth from $1.27f_c$ to $13.7f_c$ while the fabricated BPF has a -20 dB isolation bandwidth from $1.56f_0$ to $15f_0$. Moreover, the fabricated LPF and BPF also have the compact size of $0.107\lambda_{gc} \times 0.083\lambda_{gc}$ and $0.123\lambda_{g0} \times 0.073\lambda_{g0}$, respectively. Good agreement can be observed between the simulation and measurement.**

***Index Terms*—Bandpass filter (BPF), lowpass filter (LPF), radial stub, ultra-wide stopband, wideband.**

I. Introduction

MINIATURIZED lowpass filters (LPFs) and bandpass filters (BPFs) with broad stopband are in great demand for modern communication systems to transmit the desired signals in the passband and suppress harmonics and spurious signals in the stopband.

So far, various structures have been proposed to implement good lowpass performance [1]–[4]. All LPFs reported in [1]–[4] achieve greater than ten times harmonic suppression and good in-band performance. However, the LPFs presented in [1], [2] suffer from large circuit sizes. Besides, all these LPFs employ multiple resonators, resulting in complex design procedures. Therefore, it is significant for radio-frequency (RF) designers to exploit a LPF with simple physical topology, miniaturized size and broad stopband.

Moreover, high data-rate communication systems require wideband BPFs with broad stopband to improve the RF front end performance. The wideband BPFs in [5]–[8] are reported to achieve such goals, and they exhibit their own merits. However, it has to admit that these BPFs suffer from many drawbacks, i.e., large circuit size [5], etched ground planes [5]–[8] and less than five times harmonic suppression [7], [8]. The cascade of LPF and highpass filter (HPF) is a classic method to realize wideband performance. Nevertheless, such a method suffers from the insertion loss (IL) and circuit area of two filters. Therefore, the emphasis of this method is to exploit miniaturized and high performance LPF and HPF.

The motivation of this letter is to design a miniaturized LPF with simple physical topology, single-layer configuration and broad stopband. Then, such a miniaturized and high performance LPF is applied to design a cascaded LPF-HPF type wideband BPF. A section of high-impedance microstrip line (HIML), a pair of radial stubs (RSs), a pair of stepped-impedance open stubs (SIOSs) and a pair of shorted HIML are employed to realize such goals. All filters in this letter are designed on the substrate Arlon DiClad 880 ($h = 0.508$ mm, $\varepsilon_{\rm re} = 2.2$, $\tan\delta = 0.0009$). Detailed design procedure and measured results are discussed in the following sections.

II. Lowpass Filter Design

Fig. 1(a) shows a traditional three-order LPF with 0.1 dB ripple Chebyshev response and 3 dB cutoff frequency at $f_c = 1.1$ GHz. A pair of RSs loaded HIML shown in Fig. 1(b) is employed to implement such a LPF. The required value of L_1 can be controlled by the length of HIML while the required value of C_1 can be controlled by the radius and angle of RSs. The green color line with round symbol and the black color line with square symbol in Fig. 2 plots the simulated results of the traditional lumped-element three-order LPF and RSs loaded HIML, respectively. After comparison of these two lines, a transmission zero (TZ) f_z at around $7.2f_c$ and two spurious passbands at around $9.1f_c$ and $14.1f_c$ can be observed obviously in the stopband of simulated result of RSs loaded HIML. This is due to the parasitic elements of HIML and RSs. Fig. 1(c) gives a lumped-element equivalent circuit of RSs loaded HIML, which considers the parasitic elements. HIML has parasitic capacitor C_H besides L_H [9], while RS has parasitic inductors L_{R1} and L_{R2}, and parasitic capacitor C_{R2} [10]. The blue color line with triangle symbol gives the simulated result of the circuit given in Fig. 1(c), which agrees well with the simulated results of RSs loaded HIML. In practical filter design, the width of HIML is set be very narrow and a tradeoff between the radius and angle of RSs is done, so as to decrease the parasitic elements.

The RSs loaded HIML shown in Fig. 1(b) is often used as RF choke in direct current (DC) bias circuit, but it can be seen in Fig. 2 that its frequency response lacks passband selectivity and stopband rejection level when employed as an LPF. In addition, f_{sp1} around 9.1 f_c has deteriorated the stopband performance. Therefore, a pair of SIOSs are paralleled at both sides of HIML. When the one-port input impedance of SIOSs shown in Fig. 3(a)

Manuscript received March 11, 2013; revised April 27, 2013; accepted May 27, 2013. Date of publication June 27, 2013; date of current version August 05, 2013.

J. Xu, W. Wu, and C. Miao are with the Ministerial Key Laboratory of JGMT, Nanjing University of Science and Technology, Nanjing 210094, China (e-mail: xujin2njust@126.com).

Y.-X. Ji is with Xi'an Electronics Engineering Research Institute, Xi'an 710100, China

Color versions of one or more of the figures in this letter are available online at http://ieeexplore.ieee.org.

Digital Object Identifier 10.1109/LMWC.2013.2269041

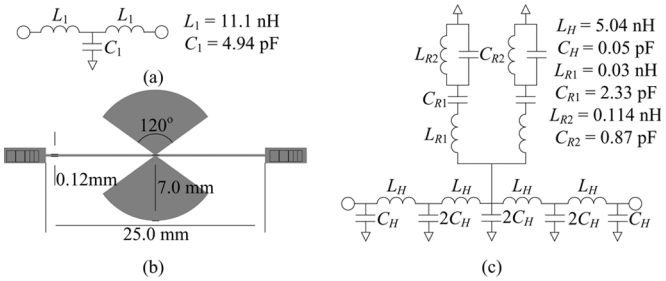

Fig. 1. (a) Traditional lumped-element three-order LPF. (b) RSs loaded HIML. (c) Lumped-element equivalent circuit of RSs loaded HIML.

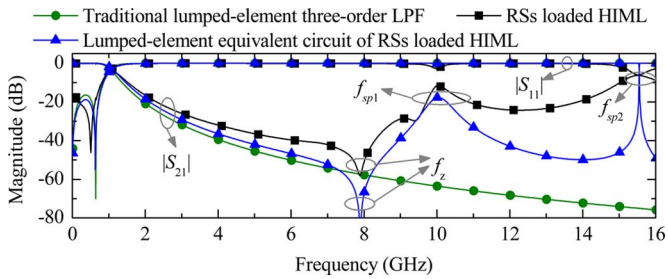

Fig. 2. Simulated results of three types of circuits given in Fig. 1.

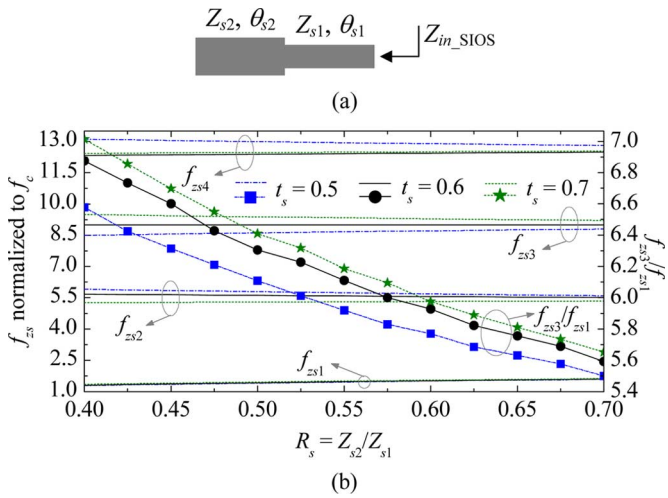

Fig. 3. (a) One-port configuration of SIOS. (b) Variation of TZs due to SIOS against different values of R_s and t_s, $Z_{s1} = 85\ \Omega$ and $(\theta_{s1} + \theta_{s2}) = 50°$ fixed.

equals to zero $(Z_{in\_SIOS} = 0)$, SIOSs can introduce a series of TZs f_{zs} which are determined by

$$Z_{s1} \tan \theta_{s1} - Z_{s2} \cot \theta_{s2} = 0. \quad (1)$$

The frequency locations of f_{zs} are mainly determined by $(\theta_{s1} + \theta_{s2})$. Fig. 3(b) depicts the variation of the first four TZs $f_{zs1} \sim f_{zs4}$ against different values of $R_s = Z_{s2}/Z_{s1}$ and $t_s = \theta_{s2}/(\theta_{s1} + \theta_{s2})$. In the LPF design, f_{zs3}/f_{zs1} close to 9.1 is the optimum value, under which f_{zs1} close to f_c can achieve the highest value of roll-off rate (ROR), and f_{sp1} canceled by f_{zs3} can extend the stopband. However, it can be seen in Fig. 3(b) that it is hard to achieve such a value. There is a compromise between ROR and the stopband bandwidth. In this letter, $R_s = 0.65$ and $t_s = 0.6$ are preset, which corresponds to $f_{zs3}/f_{zs1} = 5.6$.

According to the above discussion, Fig. 4(a) depicts final physical topology of proposed LPF. The physical dimensions

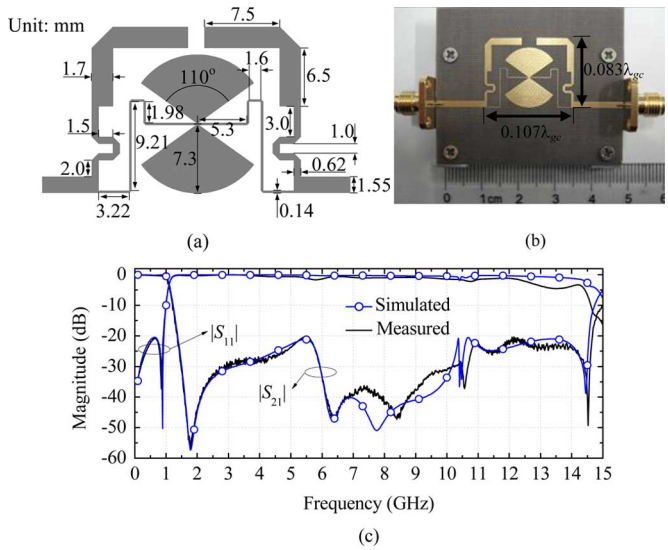

Fig. 4. (a) Physical topology, (b) photograph, and (c) simulated and measured results of proposed LPF.

TABLE I
PERFORMANCE COMPARISON WITH REPORTED LPF WITH WIDE STOPBAND

	IL (dB)	ROR (dB/octave)	Harmonic suppression	Circuit size (λ_{gc}^2)
[1]	1.0	-60	1.3 - 10.5 f_c (20 dB)	0.3 × 0.1
[2]	1.0	-144	1.14 - 13 f_c (20 dB)	0.4 × 0.16
[3]	0.39	-146	1.13 - 10.8 f_c (20 dB)	0.1 × 0.12
[4]	0.4	-39	1.55 - 16.4 f_c (15 dB)	0.11 × 0.09
This work	**0.4**	**-75**	**1.27 - 13.7 f_c (20 dB)**	**0.107 × 0.083**

of HIML, RSs and SIOSs are slightly tuned to achieve good in-band and out-of-band performance. The whole LPF structure is optimized by 3-D full-wave EM simulator HFSS. The tuned physical dimensions are labeled in Fig. 4(a). Fig. 4(b) gives the photograph of fabricated LPF, where λ_{gc} represents the guided wave-length of a 50 Ω microstrip line on the used substrate at f_c.

Fig. 4(c) plots the measured and the simulated S -parameters. The measured results are extracted by Agilent VNA 8722ES, which is calibrated by open-short-through technique. The measured results include the impact of I/O SMA connectors, and the ILs of two SMA connectors are less than 0.1 dB. The measured 3 dB cutoff frequency f_c is at 1.07 GHz. The IL in the passband is less than 0.4 dB, and the in-band return loss is better than 20 dB. Due to the SIOSs, a transmission zero is close to the passband, resulting in a sharp ROR up to -75 dB/octave. It can be also found in Fig. 4(c) that the upper stopband are suppressed to below 20 dB from $1.27f_c$ to $13.7f_c$. Table I gives a performance comparison of proposed LPF with reported works. As seen, the proposed LPF exhibits great advantages in term of electrical performance and circuit area. In addition, the proposed LPF also has the merits of simple physical topology and single-layer configuration.

III. BANDPASS FILTER DESIGN

Fig. 5 plots a simulated result of a 50 Ω microstrip line loaded with a pair of shorted HIMLs. As shown, DC and lower frequency are shorted to ground, so that it exhibits a highpass performance. Moreover, a series of TZs f_{zu} can be observed when the one-port input impedance of shorted HIML equals to zero $(Z_{ins} = 0)$. These TZs can be given by

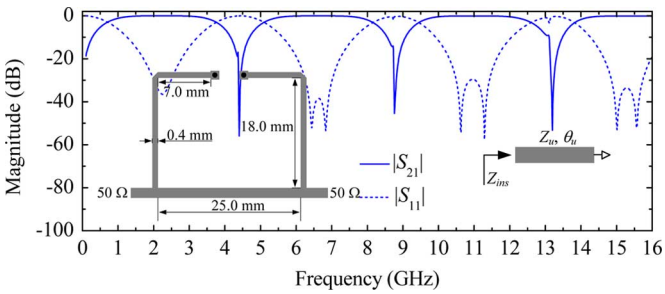

Fig. 5. Simulated result of a 50 Ω microstrip line loaded with a pair of shorted HIMLs. The insets are shorted HIMLs loaded 50 Ω microstrip line and one-port configuration of shorted HIML.

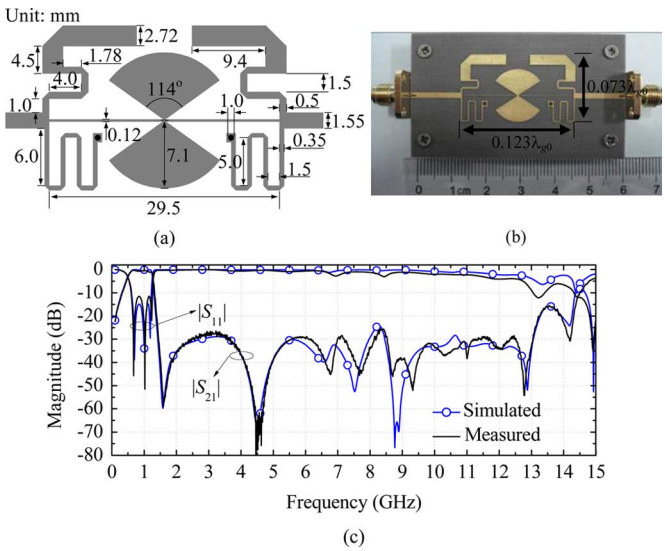

Fig. 6. (a) Physical topology, (b) photograph, and (c) simulated and measured results of proposed BPF.

TABLE II
PERFORMANCE COMPARISON WITH REPORTED WIDEBAND BPF WITH WIDE STOPBAND

	IL at f_0 (dB)	-3 dB FBW	Harmonic suppression	Circuit size (λ_{g0}^2)
[5]	1.55	69.5%	$1.37f_0$ - $6.8f_0$ (20 dB)	0.472 × 0.324
[6]	1	56.3%	$1.78f_0$ - $6.8f_0$ (30 dB)	0.235 × 0.231
[7]	0.65	59.19%	$1.5f_0$ - $4.65f_0$ (30 dB)	0.065 × 0.083
[8]	0.7	40%	$1.26f_0$ - $3.52f_0$ (15 dB)	0.294 × 0.162
[11]	0.8	110%	$1.64f_0$ - $2.4f_0$ (25 dB)	0.516 × 0.32
This Work	**0.66**	**87%**	**$1.56f_0$ - $15f_0$ (20 dB)**	**0.123 × 0.073**

$$f_{zu} = (n\pi f_0)/(\theta_u), \quad n = 1, 2, 3 \cdots \tag{2}$$

Thus, the frequency locations of f_{zu} can be easily controlled by θ_u. If θ_u is tuned to let the first f_{zu} locate at around $4.1f_c$ and the above LPF is inserted between these two shorted HIMLs, a BPF can be achieved. The higher frequencies are suppressed by LPF and the TZs introduced by shorted HIMLs can further improve the upper stopband performance of BPF.

To validate the proposed BPF design method, a wideband BPF with ultra-wide stopband is design. The shorted HIMLs are folded to achieve size reduction. Fig. 6(a) shows the physical topology of proposed BPF. The whole BPF structure is optimized by HFSS and the tuned physical dimensions are labeled in Fig. 6(a). The photograph of fabricated BPF is given in Fig. 6(b), where λ_{g0} represents the guided wave-length of a 50 Ω microstrip line on the used substrate at f_0. The simulated and measured results for the proposed BPF are plotted in Fig. 6(c). The measured results show that the fabricated filter is centered at $f_0 = 0.885$ GHz with -3 dB fractional bandwidth (FBW) of 87%. The measured IL at f_0 is around 0.66 dB and the measured return loss is better that 12 dB overall the whole passband. Measured results also show that the fabricated filter has a 20 dB rejection upper stopband from $1.56f_0$ to $15f_0$. A performance comparison of the proposed wideband BPF with some reported works is given in Table II, which also includes the authors' previous work [11]. Although two BPFs in [11] and this letter employ RSs, they have two different operating mechanisms. The radial stub loaded resonator in [11] can generate two TZs for the filter, and bandpass performance is achieved due to two coupled lines. The RSs loaded HIML in this letter exhibits lowpass performance, and BPF is designed based on the LPF-HPF concept. After comparison, it can be found that the proposed BPF has the merits of better harmonic suppression and more compact size. The proposed BPF also has the advantages of simple physical topology and single-plane configuration. Although the proposed BPF has a limited ROR in low band, it can meet most of the applications when it serves as an intermediate frequency (IF) BPF after the mixer.

IV. CONCLUSION

Based on a section of HIML, a pair of RSs, a pair of SIOSs and a pair of shorted HIMLs, this letter presents a novel LPF structure and a novel BPF structure. Two filters achieve greater than thirteen times harmonic suppression and very miniaturized size. In addition, these two filters exhibit the merits of simple physical topology, single-plane configuration and quick design procedure. Due to their excellent electrical performance and miniaturized size, these two filters are attractive in modern wireless communication systems.

REFERENCES

[1] L. Li, Z.-F. Li, and Q.-F. Wei, "Compact and selective lowpass filter with very wide stopband using tapered compact microstrip resonant cells," *Electron. Lett.*, vol. 45, no. 5, pp. 267–268, Feb. 2009.

[2] K. Ma and K. S. Yeo, "New ultra-wide stopband low-pass filter using transfromed radial stubs," *IEEE Trans. Microw. Theory Tech.*, vol. 59, no. 3, pp. 604–611, Mar. 2011.

[3] M. Hayati, H. Asadbeigi, and A. Sheikhi, "Microstrip lowpass filter with high and wide rejection band," *Electron. Lett.*, vol. 48, no. 19, pp. 1217–1219, Sep. 2012.

[4] J. P. Wang, H. Cui, and G. Zhang, "Design of compact microstrip lowpass filter with ultra-wide stopband," *Electron. Lett.*, vol. 48, no. 14, pp. 854–856, Jul. 2012.

[5] M. K. Mandal and S. Sanyal, "Design of wide-band, sharp-rejection bandpass filters with parallel-coupled lines," *IEEE Microw. Wireless Compon. Lett.*, vol. 16, no. 11, pp. 597–599, Nov. 2006.

[6] P. Mondal and A. Chakrabarty, "Compact wideband bandpass filters with wide upper stopband," *IEEE Microw. Wireless Compon. Lett.*, vol. 17, no. 1, pp. 31–33, Jan. 2007.

[7] C.-H. Liang and C. Y. Chang, "Compact wideband bandpass filters using stepped-impedance resonators and interdigital coupling structures," *IEEE Microw. Wireless Compon. Lett.*, vol. 19, no. 9, pp. 551–553, Sep. 2009.

[8] X. Luo, J.-G. Ma, and E.-P. Li, "Wideband bandpass filter with wide stopband using loaded BCMRC stub and short-stub," *IEEE Microw. Wireless Compon. Lett.*, vol. 21, no. 7, pp. 353–355, Jul. 2011.

[9] I. J. Bahl, *Lumped Element for RF and Microwave Circuits*. Norwood, MA, USA: Artech House, 2003.

[10] F. Giannini and C. Paoloni, "Broadband lumped equaivalent circuit for shunt-connected radial stub," *Eletron. Lett.*, vol. 22, no. 9, pp. 486–487, Apr. 1986.

[11] J. Xu, W. Wu, W. Kang, and C. Miao, "Compact UWB bandpass filter with a notched band using radial stub loaded resonator," *IEEE Microw. Wireless Compon. Lett.*, vol. 22, no. 7, pp. 351–353, Jul. 2012.